BIOLOGICAL SCIENCES, Neuroscience

The 190 kDa Ankyrin-G isoform is required for the dendritic stability of neurons and its palmitoylation is altered by lithium

Nicolas H. Piguel[a,g] Sehyoun Yoon[a,g] Francesca I. DeSimone[b] Shaun S. Sanders[b] Ruoqi Gao[a] Katherine E. Horan[a] Leonardo E. Dionisio[a] , Jacob C. Garza[c] Tracey L. Petryshen[c] Gareth M. Thomas[d] Katharine R. Smith[e] and Peter Penzes[a,f,g]*

[a] Department of Physiology, Northwestern University Feinberg School of Medicine, Chicago, IL 60611

[b] Shriners Hospitals Pediatric Research Center, Lewis Katz School of Medicine at Temple University, Philadelphia, PA 19140

[c] Psychiatric and Neurodevelopmental Genetics Unit, Department of Psychiatry and Center for Genomic Medicine, Massachusetts General Hospital, Harvard Medical School, Boston, MA

[d] Shriners Hospitals Pediatric Research Center and Department of Anatomy and Cell Biology, Lewis Katz School of Medicine at Temple University, Philadelphia, PA 19140

[e] Department of Pharmacology, University of Colorado School of Medicine, Aurora, CO 80045

[f] Department of Psychiatry and Behavioral Sciences, Northwestern University Feinberg School of Medicine, Chicago, IL 60611

[g] Northwestern University Center for Autism and Neurodevelopment, Chicago, IL 60611

*Corresponding author: Department of Physiology, Northwestern University Feinberg School of Medicine, Chicago, IL 60611; Tel: 312-503-5379; p-penzes@northwestern.edu

***ANK3* | ankyrin-G | dendrite | dendritic spine | palmitoylation | lithium**

Abstract

The *ANK3* gene, which encodes ankyrin-G (AnkG), is associated with a variety of neuropsychiatric and cognitive disorders including bipolar disorder, autism spectrum disorder, and schizophrenia. These diseases are characterized by abnormal dendritic and synaptic architecture. AnkG is a multifunctional scaffold protein with several isoforms: The 480 kDa and 270 kDa isoforms have roles at the axon initial segment and node of Ranvier, but the function of the 190 kDa isoform (AnkG-190) is less well understood. Moreover, AnkG isoforms are regulated by palmitoylation, but palmitoylation of AnkG-190 has not been investigated in neurons. Here we show that AnkG is required for normal dendrite and spine architecture in vivo and that AnkG-190 stabilizes pyramidal neuron dendrites. We found that palmitoylation at Cys70 stabilizes AnkG-190 in spine heads and at dendritic plasma membrane nanodomains. Finally, we found that lithium, a commonly used mood stabilizer, reduces AnkG-190 palmitoylation and increases its mobility in spines by inhibiting ZDHHC8 action. Taken together, our data reveal a novel mechanism regulating dendritic architecture and mood stabilizer action on palmitoylation of an important psychiatric disorder risk factor.

Significance

The *ANK3* gene has been associated with bipolar disorder and schizophrenia although the mechanisms of disease are not known. The AnkG 190 kDa isoform, AnkG-190, was previously described for its role in dendritic spines. Here, we show it is required to stabilize dendritic arborization and show that palmitoylation, a post-translation modification which allows proteins to stabilize at the membrane, is critical for its localization. Moreover, we show that lithium, a mood stabilizer commonly used in bipolar disorder, modifies AnkG-190 palmitoylation and its dendritic spine localization by inhibiting ZDHHC8 activity, another protein encoded by a psychiatric disorder risk gene. We describe a new novel function for Ank-190 and the early mechanistic actions of lithium in neurons.

Introduction

The human *ANK3* gene, encoding ankyrin-G (AnkG), has been associated with various neuropsychiatric diseases, including bipolar disorder (BD), schizophrenia, and autism spectrum disorder (ASD) (1-3). Multiple independent genome wide association studies (GWAS) have strongly linked *ANK3* to BD in a variety of different ethnicities (4-7) and have been corroborated by meta-analyses (8). In addition to a genetic association with *ANK3*, some studies have shown an increase of *ANK3* expression in blood (9) and in lymphoblastoid cells of BD patients (10), revealing a potential disease mechanism. Furthermore, a BD-related risk variant in *ANK3* was associated with decreased expression of a specific AnkG isoform in the cerebellum (11) and variants linked to loss of function are also implicated in ASD and ID (12). Thus, either increases or decreases of *ANK3* gene expression and isoform specific variation may be implicated in disease.

The *ANK3* gene encodes multiple isoforms of AnkG, of which the 190, 270, and 480 kDa isoforms are the most prominent in brain (13). The giant 270 and 480 kDa isoforms have been mostly studied for their function in the axon initial segment (AIS) (14) or in nodes of Ravier (15), but the 480 kDa isoform has also been shown to prevent gamma-aminobutyric acid (GABA) receptor endocytosis and to have an important role in maintaining GABAergic synapses (16). The role of the 190 kDa isoform (AnkG-190) is less fully described in neurons, but it can be found in human postsynaptic density (PSD) fraction, where it decreases in BD (17). Moreover, AnkG-190 was found to increase in rat PSD after 5 weeks of lithium treatment (18). AnkG-190 seems to play an important role in dendritic spine maintenance and long-term potentiation through subsynaptic nanodomains in dendritic spine heads and necks (19). Given its role in dendritic spines and that BD and schizophrenia are highly correlated to a decreases of dendritic spines and dendrites (20) (21), we reasoned that AnkG-190 may regulate dendrite architecture. However, its function in dendrites has not yet been studied and the regulation of its localization in dendrites and synapses, are not known.

A critical process in the stabilization of proteins in dendritic spines and dendrites is S-palmitoylation, a reversible form of post-translational modification regulating protein attachment to lipid membranes (22) and localizing proteins to different neuronal subcompartments (23). Important synaptic proteins, including neurotransmitter receptors, scaffold proteins, transporters, adhesion molecules, SNAREs, and other trafficking proteins, are palmitoylated (24) and palmitoylation also regulates dendrite and synapse morphology (25). However, little is known about the role of palmitoylation in dendrite stability and how it is altered by therapeutic agents.

The membrane-binding regions of all three main AnkG isoforms harbor a cysteine residue (C70) that can be palmitoylated, a process that is required for AnkG association with the membrane, appropriate cellular localization, and function in non-neuronal cells (26, 27). Structural analysis has shown that the membrane anchoring of AnkG is facilitated by palmitoylation, defining a stable binding interface on the lipid membrane (28). Interestingly, non-palmitoylated AnkG also localized near the membrane but lacked a unique binding interface. Palmitoylation is known to play an important role in the function of 270 and 480 kDa isoforms, but the role of palmitoylation of the 190 kDa isoform in neurons is unknown (16, 26).

Lithium is a mood stabilizer commonly used to treat BD patients as a first-line intervention (29). It has been show than lithium can regulate localization of proteins at the synapse (30). Responsiveness of BD patients to lithium treatment appears to be a heritable trait (31) linked to genetic markers in patients isolated from GWAS (32). The identification of single nucleotide polymorphisms within the *ANK3* regulatory region associated to lithium response suggest that AnkG may be involved in lithium-dependent pathways (33) but a little is known about the effect of lithium on the protein's localization and function. Because understanding of synaptic palmitoylation is likely to provide insights into normal neuronal function but also pathophysiological and therapeutic mechanisms (34), we investigated the physiological function of AnkG palmitoylation and its roles in the actions of lithium. We show that AnkG-190 stabilizes pyramidal neuronal basal dendrites and that Palmitoylation stabilizes AnkG-190 in spines and at dendritic plasma membrane nanodomains. Finally, lithium reduces AnkG-190 palmitoylation and increases its mobility in spines in a ZDHHC8-dependent-pathway. Taken together, our data reveal a new role for AnkG-190 in dendritic architecture and a novel mechanism of lithium action on AnkG-190 palmitoylation.

Results

AnkG-190 maintains dendrite complexity in pyramidal neurons. We have previously shown that AnkG-190 has an essential role in dendritic spine maintenance in vitro (19), but whether AnkG is similarly important in vivo has not been addressed. To investigate this question, we performed Golgi-Cox staining in *Ank3* cKO (*Ank3*$^{flox/flox}$, *Camk2a*-Cre) mouse brain slices. In this model, Cre recombinase is expressed under a *Camk2a* promoter to target the *Ank3* gene in the postnatal forebrain (*SI Appendix*, Fig. S1A) (35), a critical period for dendritic spine formation, and leading to a decrease of the AnkG-190. We analyzed dendrites of pyramidal neurons from layer 2/3 of the somatosensory cortex, a region of the cortex where AnkG is abundant and where we saw a decrease of expression in neurons (Fig. S1C-D). Quantitative analysis of spine number showed a decrease in spine density in *Ank3* cKO brains, in support of our previous in vitro findings (Fig. 1B, E and G). We also observed that *Ank3* cKO mice had striking alterations in dendrite morphology with decrease in basal dendrite complexity (Fig. 1C, F and H).

To specifically determine whether the effects in dendrites were cell-autonomous, we knocked down AnkG expression in rat primary cortical neurons using an *Ank3* RNAi we previously described (19). By separating apical and basal dendrites (see supplementary methods), we again found reduced complexity in the basal dendritic arbor of AnkG knockdown pyramidal neurons (Fig. 1IJ and K), with no change in apical dendrites (Fig. 1L). Interestingly, coexpression of an RNAi-resistant AnkG-190 construct restored dendritic complexity, whereas coexpression of an RNAi-resistant 270 kDa isoform did not (Fig. 1K), reminiscent of our previous observations in spines (19). Notably, AnkG knockdown also reduces dendrite complexity of interneurons, but this effect is only partially rescued by the overexpression of AnkG-270, and cannot be rescued by AnkG-190, suggesting isoform-specific requirements for different neuronal subtypes (*SI Appendix*, Fig. S1A, B). Together, these data indicate that the AnkG-190 isoform may have a specific role in maintaining basal dendrite complexity of cortical pyramidal neurons in addition to maintaining spine morphogenesis (19).

Palmitoylation of C70 stabilizes AnkG-190 in dendritic spine head and dendritic nanodomains. The specific role of AnkG-190 in dendritic spine and dendrite maintenance led us to ask what post-translational modifications would regulate these specific functions of AnkG-190. Because palmitoylation is a general mechanism for regulation of synaptic proteins, and palmitoylation of AnkG-190 in non-neuronal cells was shown to be essential for the association of AnkG with plasma membranes (26-28), we hypothesized that this modification may also modulate AnkG-190's regulation in dendrites. We first validated the presence of palmitoylated

AnkG-190 in rat cortex utilizing the acyl-biotinyl exchange assay (see supplementary methods) (26), which exchanges palmitoyl modifications with biotin (Fig. 2A). We therefore mutated the palmitoylated residue (26) to alanine (C70A) in a GFP fusion construct (GFP-AnkG-190-C70A) to assess how palmitoylation-deficient AnkG-190 would localize in neuronal dendrites and spines (Fig. 2B).

Confocal images revealed that overexpressed GFP-AnkG-190 is enriched in the spine head, as previously observed (19), and this enrichment is lost when C70A was mutated, matching the levels of soluble GFP (Fig. 2C and D). To access localization on AnkG-190-C70A of dendritic spines, we used super-resolution structured illumination microscopy (SIM) imaging (19, 36). Dendritic spine imaging confirm the confocal data. AnkG-190-C70A seems to prevent formation of nanodomains present in the spine head observed in the AnkG-190 condition (Fig. 2E). SIM imaging of dendrites showed that the C70A point mutation did not alter the presence of AnkG-190 at the membrane, but changed its localization pattern (Fig. 2F). We found that AnkG-190-C70A has a more diffuse distribution pattern compared to AnkG-190 (Fig. 2F and G) measured by a smaller variation in fluorescence intensity (Puncta index), suggesting palmitoylation is important to maintain nanodomains along the dendrite.

Lithium reduces AnkG-190 palmitoylation and increases its mobility. Lithium treatment has been shown to alter the localization of proteins in neurons (30), therefore we reasoned that it may have an effect on palmitoylation, a key post-translational mechanism to affecting subcellular localization. To investigate lithium-dependent modifications of AnkG, we performed an ABE assay in cortical neuron cultures followed by western blotting of AnkG. Interestingly, treatment with lithium resulted in a ~58% decrease in palmitoylated AnkG-190 (Fig. 3A, B) which reach levels similar to the control condition containing the palmitoylation inhibitor 2-Bromopalmitate. Interestingly, lithium was not able to reduce GRIP1 palmitoylation (*SI Appendix*, Fig S3A and B), another protein present in dendritic spines. Consistent with a reduction in palmitoylation, immunocytochemistry of cortical neuron cultures after lithium treatment revealed a decrease in endogenous AnkG staining in mature spines (width ≥0.8 μm), which contain higher levels of AnkG (19), compared to vehicle treatment (Fig. 3C, D). These data demonstrate that lithium reduces the amount of AnkG localized in spines, which is consistent with the localization of palmitoylation-deficient AnkG. This result led us to hypothesize that lithium could prevent palmitoylation of AnkG-190 and therefore increase AnkG mobility in spines. To test this hypothesis, we performed fluorescence recovery after photobleaching (FRAP) in neurons overexpressing AnkG-190 and treated with lithium for 24 h (Fig. 3E-G). Interestingly, lithium treatment increased the mobile

fraction of AnkG-190 from ~52% to ~75% (Fig. 3G). This level is comparable to the AnkG-190-C70A which cannot be palmitoylated, and supports an effect of lithium on the reduction of AnkG-190 palmitoylation leading to an increase of its mobility.

Lithium prevents DHHC8 to stabilize AnkG-190 in dendritic spines. Next, we investigated which palmitoyl acyl transferases (PATs) could regulate AnkG-190 mobility in the spine. PATs which have the capability of palmitoylating AnkG have been described in HEK293 and MDCK cells and include ZDHHC5 and ZDHHC8 that target the C70 residue on AnkG-190 (27). By using overexpression and FRAP imaging in neuron cultures, we verified if ZDHHC5 and ZDHHC8 were able to stabilize AnkG-190 in dendritic spines and if lithium was capable of reversing the process. To ensure that the effects of palmitoylation were specifically measured, we treated cultures with Palmostatin B, an inhibitor of thioesterase APT1 and APT2 (37), blocking the depalmitoylation pathway. We found that ZDHHC5 did not affect the recovery of fluorescence of GFP-AnkG-190 (Fig. 4A-C) demonstrating that it does not modulate AnkG-190 mobility in spines. In contrast, ZDHHC8 significantly decreased the GFP-AnkG-190 mobile fraction in the dendritic spine (Fig. 4A, D and E), suggesting it can palmitoylate AnkG-190 and stabilize the protein in the dendritic spine. Moreover, we found that lithium treatment can inhibit the effects of ZDHHC8 overexpression on GFP-AnkG-190 confirming its action on the palmitoylation process.

Discussion

In this study, we demonstrate a role for AnkG-190 in the arborization of pyramidal neuronal dendrites and dendritic spine density in vivo. Multiple *Ank3* KO mouse models have severe behavioral deficits related to psychiatric disorders (35, 38). Our data support that those phenotypes may, at least in part, depend on alterations of dendrite and spine architecture. Interestingly, reduced dendritic length and spine density have already been described in BD patient brain tissue in post-mortem studies (20) and in iPSCs (21). Together these observations suggest that altered neuronal morphology has an central role in neuropsychiatric diseases (39).We identify the AnkG-190 isoform as being specifically required for the cell-autonomous maintenance of basal dendrite arborization in pyramidal neurons, as the 270 kDa form is unable to rescue arborization deficits caused by knockdown of all AnkG isoforms. This phenotype can be due the specific localization of isoforms since AnkG-190 is enriched in dendrites whereas AnkG-270 is enriched in axon (19). We show that AnkG palmitoylation has a dendritic subcompartments-specific role, as it affects only basal but not apical dendrites. This may have implications for pathogenesis of *ANK3-deficit*-related disorders and bipolar disorder, as basal dendrites receive different inputs, integrate distinct signals, and are selectively regulated in physiological, as

compared to apical ones (20, 40). In addition, loss of AnkG also affects interneuron dendrites, but this dependence relies on other AnkG isoforms, indicating the cell-type specificity of AnkG-190.

We show here that AnkG-190 is palmitoylated in brain tissue, and that this modification is important for AnkG-190 subcellular localization to dendrites and spines. We don't lose AnkG-190 localization at the membrane or in the dendritic spine neck suggesting AnkG-190 can be stabilize by some protein partner interactions like spectrin (19). However, nanodomains in spine head and dendrites seem to disappear with a diffuse staining along the dendrite membrane. Unpalmitoylated AnkG has a higher mobility within spines, indicating that palmitoylation restricts its mobility to specific sites, but still conserve a smaller stable population. These data suggest that only a subset of AnkG is palmitoylated at Cystein 70 and other subpopulations of AnkG-190 exist in spines with distinct roles.

Lithium is commonly used for the treatment of mood disorders and may therefore regulate proteins genetically linked to pathophysiology such as *ANK3*. Analysis of functional SNPs from GWAS data suggest that AnkG may be involved in the lithium response (33). Lithium has been shown to rescue some BD-related behavioral deficits in different *Ank3* KO mouse model (35, 41, 42), suggesting it can alleviate symptoms of mouse models with AnkG loss of function. However, heterozygous and homozygous loss of ANK3 likely represent rare mutations only present in a small subset of patients with ASD and ID, and the majority of individuals with BD are likely to retain AnkG expression or have increased expression (9, 10, 43). Moreover, KO of exon 37 targeting 270 kDa and 480 kDa isoform induce a fivefold expression increase of AnkG-190 isoform (44). Therefore AnkG-dependent mechanisms may also play a role in the lithium response

Only ZDHHC8, one of the two PATs described to palmitoylate AnkG-190 (26), can stabilize GFP-AnkG-190 in dendritic spine when we overexpressed it. This effect is abolish after 24 hour lithium stimulation supporting the decrease of AnkG-190 palmitoylation is due to the inhibition of ZDHHC8 activity. Moreover, palmitoylated GRIP1, which is a target of ZDDHC8 too (26), is not decrease during lithium treatment indicating a specific inhibition of AnkG-190 palmitoylation.

In summary, we present evidence for a novel mechanism of dendritic architecture controlled by the AnkG-190 isoform. Our work describes a new mechanism of mood stabilizer action and its effects on an important psychiatric disorder risk factor *ANK3*. These findings open new directions for understanding basic control of neuroarchitecture, but may also provide new opportunities for treatment.

Materials and Methods

Detailed materials and methods can be found in *SI Appendix*, *SI Materials and Methods*.

Conditional KO mice: *Ank3*-floxed mice (*Ank3*$^{flox/flox}$) (The Jackson Laboratory; Bar Harbor, ME, USA; #029797) were crossed with *Camk2a*-Cre mice (The Jackson Laboratory; #005359) for forebrain-specific homozygous deletion of *Ank3* (*Ank3*$^{flox/flox}$, *Camk2a*-cre). The resulting mouse strain was called *Ank3* cKO. To maintain the colonies, *Ank3* cKO mice were mated with *Ank3*$^{flox/flox}$ mice. All experiments were performed following protocols approved by the Institutional Animal Care and Use Committee at Northwestern University.

Pharmacological treatments: 2-Bromopalmitate (2-BrP), a palmitoylation inhibitor, and S-methyl methanethiosulfonate (MMTS), a thiol blocker, were from Sigma (St. Louis, MO, USA). All other chemicals were from ThermoFisher Scientific (Waltham, MA, USA) and were of the highest reagent grade. 2-BrP was used at 20 mM, palmostatin B (which inhibits depalmitoylation) at 50 μM, lithium chloride at 2 mM, and all were applied for stimulation over 24 h.

Acyl biotinyl exchange assay: For acyl biotinyl exchange (ABE) experiments, rat cortical neurons cultured as described above were lysed directly in buffer (50 mM HEPES pH 7.0, 2% SDS, 1 mM EDTA plus protease inhibitor mixture (PIC, Roche) and 20 mM MMTS (to block free thiols). Following lysis, excess MMTS was removed by acetone precipitation. Pellets were dissolved in buffer containing 4% (wt/vol) SDS. Samples were diluted and incubated for 1 h in either 0.7 M hydroxylamine (NH2OH) pH 7.4 (to cleave thioester bonds) or 50 mM Tris pH 7.4, both containing sulfhydryl-reactive (HPDP-) biotin, and incubated for 1 h at room temperature. Acetone precipitation was performed to remove unreacted HPDP-biotin and hydroxylamine and pellets were resuspended in lysis buffer without MMTS. SDS was diluted to 0.1% (wt/vol) and biotinylated proteins in the samples were affinity-purified using neutravidin-conjugated beads. Beta-mercaptoethanol [1% (vol/vol)] was used to cleave HPDP-biotin and release purified proteins from the beads. The released proteins in the supernatant were denatured in SDS sample buffer and processed for SDS-PAGE. Adult rat forebrain was dissected, rapidly cooled in ice-cold recording buffer (26) and homogenized in 10 volumes of 4 mM HEPES, 320 mM sucrose, pH 7.4, containing fresh PIC and 20 mM MMTS. Samples were centrifuged to remove debris, brought to room temperature, and SDS was added to 1% (v/v) final concentration. Samples were then centrifuged at 27,000 x *g* for 30 min at 4°C and supernatants subjected to acetone precipitation and ABE as described above.

Fluorescence recovery after photobleaching: Neurons were imaged at 37°C, 5% CO_2, with a Nikon C2 confocal microscope using a 63x oil immersion objective with NA = 1.4 in an OKOLAB stage-type CO_2 incubator. Single plane images were captured with an EMCCD camera every 10 s for 200 s. 80% laser power pulses of 1 ms (2 iterations) were used to bleach GFP in the spine. After background subtraction and validation of maximum 10% remaining fluorescence after photobleaching, data were normalized with the prebleach value. Recovery data points were then fitted to a one-phase association exponential in GraphPad Prism. The mobile fraction was calculated as an average of the plateaued fluorescence level and expressed as a percentage of the pre-bleached level.

Statistical analysis; All statistical tests were performed with GraphPad Prism. Data were tested for normality with D'Agostino and Pearson methods to determine use of non-parametric (Mann-Whitney, Kruskal-Wallis, Spearman correlations) or parametric (unpaired t-test, ANOVA, Pearson correlations) tests. Post-hoc tests were included in analyses with multiple comparisons. Bar graphs the mean ± SEM, unless otherwise noted. Differences were considered significant if $p \leq 0.05$. N values refer to number of cells per condition, unless otherwise stated.

Footnotes

*To whom correspondence should be addressed. Email: p-penzes@northwestern.edu

Author contributions: N.H.P., S.Y., F.I.D., S.S.S., G.M.T. and P.P. designed research; N.H.P., S.Y., F.I.D., S.S.S., R.G., K.E.H., L.E.D. and K.R.S. performed research; N.H.P., S.Y., F.I.D., S.S.S. analyzed data; N.H.P., S.Y., F.I.D., S.S.S., J.S.T., T.L.P., K.R.S, G.M.T. and P.P. wrote the paper.

The authors declare no competing interests.

Acknowledgments

This work was supported by R01MH107182 to P.P. Imaging work was performed at the Northwestern University Center for Advanced Microscopy, generously supported by NCI CCSG P30 CA060553 awarded to the Robert H. Lurie Comprehensive Cancer Center. We are grateful to members of the Penzes lab for helpful discussions, especially Dr. Marc P. Forrest for his help on the manuscript. Dr. Antonio Sanz-Clemente is gratefully acknowledged for providing access to his lab equipment. We thank Dr. Shernaz Bamji for sharing plasmid. All experiments involving animals were performed according to the Institutional Animal Care and Use Committee of NU.

References

1. Bi C*, et al.* (2012) Mutations of ANK3 identified by exome sequencing are associated with autism susceptibility. *Hum Mutat* 33(12):1635-1638.
2. Yuan A*, et al.* (2012) ANK3 as a risk gene for schizophrenia: new data in Han Chinese and meta analysis. *Am J Med Genet B Neuropsychiatr Genet* 159B(8):997-1005.
3. Schulze TG*, et al.* (2009) Two variants in Ankyrin 3 (ANK3) are independent genetic risk factors for bipolar disorder. *Mol Psychiatry* 14(5):487-491.
4. Scott LJ*, et al.* (2009) Genome-wide association and meta-analysis of bipolar disorder in individuals of European ancestry. *Proc Natl Acad Sci U S A* 106(18):7501-7506.
5. Smith EN*, et al.* (2009) Genome-wide association study of bipolar disorder in European American and African American individuals. *Mol Psychiatry* 14(8):755-763.
6. Tesli M*, et al.* (2011) Association analysis of ANK3 gene variants in nordic bipolar disorder and schizophrenia case-control samples. *Am J Med Genet B Neuropsychiatr Genet* 156B(8):969-974.
7. Muhleisen TW*, et al.* (2014) Genome-wide association study reveals two new risk loci for bipolar disorder. *Nat Commun* 5:3339.
8. Roby Y (2017) ANK3 gene polymorphisms and bipolar disorder: a meta-analysis. *Psychiatr Genet* 27(6):225-235.

9. Wirgenes KV*, et al.* (2014) ANK3 gene expression in bipolar disorder and schizophrenia. *Br J Psychiatry* 205(3):244-245.
10. Kato T, Hayashi-Takagi A, Toyota T, Yoshikawa T, & Iwamoto K (2011) Gene expression analysis in lymphoblastoid cells as a potential biomarker of bipolar disorder. *J Hum Genet* 56(11):779-783.
11. Rueckert EH*, et al.* (2013) Cis-acting regulation of brain-specific ANK3 gene expression by a genetic variant associated with bipolar disorder. *Mol Psychiatry* 18(8):922-929.
12. Iqbal Z*, et al.* (2013) Homozygous and heterozygous disruptions of ANK3: at the crossroads of neurodevelopmental and psychiatric disorders. *Hum Mol Genet* 22(10):1960-1970.
13. Zhang X & Bennett V (1998) Restriction of 480/270-kD ankyrin G to axon proximal segments requires multiple ankyrin G-specific domains. *J Cell Biol* 142(6):1571-1581.
14. Leterrier C & Dargent B (2014) No Pasaran! Role of the axon initial segment in the regulation of protein transport and the maintenance of axonal identity. *Semin Cell Dev Biol* 27:44-51.
15. Nelson AD & Jenkins PM (2017) Axonal Membranes and Their Domains: Assembly and Function of the Axon Initial Segment and Node of Ranvier. *Front Cell Neurosci* 11:136.
16. Tseng WC, Jenkins PM, Tanaka M, Mooney R, & Bennett V (2015) Giant ankyrin-G stabilizes somatodendritic GABAergic synapses through opposing endocytosis of GABAA receptors. *Proc Natl Acad Sci U S A* 112(4):1214-1219.
17. Focking M*, et al.* (2016) Proteomic analysis of the postsynaptic density implicates synaptic function and energy pathways in bipolar disorder. *Transl Psychiatry* 6(11):e959.
18. Nanavati D*, et al.* (2011) The effects of chronic treatment with mood stabilizers on the rat hippocampal post-synaptic density proteome. *J Neurochem* 119(3):617-629.
19. Smith KR*, et al.* (2014) Psychiatric risk factor ANK3/ankyrin-G nanodomains regulate the structure and function of glutamatergic synapses. *Neuron* 84(2):399-415.
20. Konopaske GT, Lange N, Coyle JT, & Benes FM (2014) Prefrontal cortical dendritic spine pathology in schizophrenia and bipolar disorder. *JAMA Psychiatry* 71(12):1323-1331.
21. Tobe BTD*, et al.* (2017) Probing the lithium-response pathway in hiPSCs implicates the phosphoregulatory set-point for a cytoskeletal modulator in bipolar pathogenesis. *Proc Natl Acad Sci U S A* 114(22):E4462-E4471.
22. Salaun C, Greaves J, & Chamberlain LH (2010) The intracellular dynamic of protein palmitoylation. *J Cell Biol* 191(7):1229-1238.
23. Tortosa E & Hoogenraad CC (2018) Polarized trafficking: the palmitoylation cycle distributes cytoplasmic proteins to distinct neuronal compartments. *Curr Opin Cell Biol* 50:64-71.
24. Kang R*, et al.* (2008) Neural palmitoyl-proteomics reveals dynamic synaptic palmitoylation. *Nature* 456(7224):904-909.
25. Shah BS, Shimell JJ, & Bamji SX (2019) Regulation of dendrite morphology and excitatory synapse formation by zDHHC15. *J Cell Sci* 132(13).
26. Thomas GM, Hayashi T, Chiu SL, Chen CM, & Huganir RL (2012) Palmitoylation by DHHC5/8 targets GRIP1 to dendritic endosomes to regulate AMPA-R trafficking. *Neuron* 73(3):482-496.
27. He M, Abdi KM, & Bennett V (2014) Ankyrin-G palmitoylation and betaII-spectrin binding to phosphoinositide lipids drive lateral membrane assembly. *J Cell Biol* 206(2):273-288.
28. Fujiwara Y*, et al.* (2016) Structural basis for the membrane association of ankyrinG via palmitoylation. *Sci Rep* 6:23981.
29. Malhi GS, Gessler D, & Outhred T (2017) The use of lithium for the treatment of bipolar disorder: Recommendations from clinical practice guidelines. *J Affect Disord* 217:266-280.
30. Farooq M*, et al.* (2017) Lithium increases synaptic GluA2 in hippocampal neurons by elevating the delta-catenin protein. *Neuropharmacology* 113(Pt A):426-433.

31. Grof P*, et al.* (2002) Is response to prophylactic lithium a familial trait? *J Clin Psychiatry* 63(10):942-947.
32. Hou L*, et al.* (2016) Genetic variants associated with response to lithium treatment in bipolar disorder: a genome-wide association study. *Lancet* 387(10023):1085-1093.
33. Higgins GA, Allyn-Feuer A, Barbour E, & Athey BD (2015) A glutamatergic network mediates lithium response in bipolar disorder as defined by epigenome pathway analysis. *Pharmacogenomics* 16(14):1547-1563.
34. Thomas GM, Hayashi T, Huganir RL, & Linden DJ (2013) DHHC8-dependent PICK1 palmitoylation is required for induction of cerebellar long-term synaptic depression. *J Neurosci* 33(39):15401-15407.
35. Zhu S*, et al.* (2017) Genetic disruption of ankyrin-G in adult mouse forebrain causes cortical synapse alteration and behavior reminiscent of bipolar disorder. *Proc Natl Acad Sci U S A* 114(39):10479-10484.
36. Crosby KC*, et al.* (2019) Nanoscale Subsynaptic Domains Underlie the Organization of the Inhibitory Synapse. *Cell Rep* 26(12):3284-3297 e3283.
37. Rusch M*, et al.* (2011) Identification of acyl protein thioesterases 1 and 2 as the cellular targets of the Ras-signaling modulators palmostatin B and M. *Angew Chem Int Ed Engl* 50(42):9838-9842.
38. Liu C*, et al.* (2017) AnkG hemizygous mice present cognitive impairment and elevated anxiety/depressive-like traits associated with decreased expression of GABA receptors and postsynaptic density protein. *Exp Brain Res* 235(11):3375-3390.
39. Forrest MP, Parnell E, & Penzes P (2018) Dendritic structural plasticity and neuropsychiatric disease. *Nat Rev Neurosci* 19(4):215-234.
40. Srivastava DP*, et al.* (2012) An autism-associated variant of Epac2 reveals a role for Ras/Epac2 signaling in controlling basal dendrite maintenance in mice. *PLoS Biol* 10(6):e1001350.
41. Gottschalk MG*, et al.* (2017) Lithium reverses behavioral and axonal transport-related changes associated with ANK3 bipolar disorder gene disruption. *Eur Neuropsychopharmacol* 27(3):274-288.
42. Leussis MP*, et al.* (2013) The ANK3 bipolar disorder gene regulates psychiatric-related behaviors that are modulated by lithium and stress. *Biol Psychiatry* 73(7):683-690.
43. Hughes T*, et al.* (2018) Elevated expression of a minor isoform of ANK3 is a risk factor for bipolar disorder. *Transl Psychiatry* 8(1):210.
44. Jenkins PM*, et al.* (2015) Giant ankyrin-G: a critical innovation in vertebrate evolution of fast and integrated neuronal signaling. *Proc Natl Acad Sci U S A* 112(4):957-964.

Figure Legends

Figure 1. The AnkG-190 isoform maintains dendrite complexity in pyramidal neurons. (**A-H**) Bright field images of Golgi-Cox staining in somatosensory cortical slices from (**A**) wild-type (WT) and (**D**) Ank3 cKO 12-weeks mice, scale=100 µm. Dendrite pictures (**B** and **E**, scale=5 µm) and representative traces of basal dendrites (**C** and **F**, scale=20 µm) from pyramidal neurons from cortical layer 2/3 (**G**) Scatter plot of spine density from WT and AnkG cKO mice (46 cells, 3 brains per group, t-test, ± SEM, ***$p \leq 0.001$). (**H**) Graph showing Sholl analysis for basal dendrites (20 neurons, 3 brains per group, 2-way ANOVA with Dunnett's post-test, *$p \leq 0.05$, **$p \leq 0.01$, ***$p \leq 0.001$, ±SEM. (**I**) Representative traces of 24-days cultured rat neurons expressing for 3 days scramble or AnkG RNAi with GFP (no AnkG), GFP-AnkG-190, mCherry-AnkG-270. Scale=100 µm. (**J-L**) Graphs showing Sholl analysis for total (**J**), basal (**K**), and apical (**L**) dendrites (15-22 neurons, 2-way ANOVA with Dunnett's post-test, *$p \leq 0.05$, **$p \leq 0.01$, ***$p \leq 0.001$, ±SEM).

Figure 2. Palmitoylation of cysteine 70 stabilizes AnkG-190 in dendritic spines and dendrites. (**A**) AnkG-190 is palmitoylated in rat forebrain. Solubilized rat forebrain homogenates were subjected to ABE to purify palmitoylated proteins. ABE fractions and a portion of input homogenate (Inp.) were western blotted to detect AnkG. Exclusion of NH_2OH was used as a control for assay specificity. (**B**) Schematic of 190 kDa Ankyrin-G isoform showing the mutated cysteine which prevents palmitoylation. (**C**) Confocal images of 24 day cultured cortical neurons expressing mCherry with GFP, GFP-AnkG-190, or GFP-AnkG-190-C70A for 1 days, scale=5 µm. (**D**) Linescan analysis of spine:dendrite ratio of expressed GFP, GFP-AnkG-190, or GFP-AnkG-190-C70A (16-20 neurons per condition, 2-way ANOVA with Dunnett's post-test, ***$p \leq 0.001$, ±SEM). (**E**) Spine SIM imaging 3D reconstruction of cultured rat neurons expressing mCherry (white), GFP-AnkG-190 or GFP-AnkG-190-C70A (both green), scale=0.5 µm. (**F**) SIM imaging of dendrites from cultured cortical neurons expressing GFP-AnkG-190 or GFP-AnkG-190-C70A, scale=0.5 µm, in gray or pseudocolor (middle and bottom) and their associated normalized linescan (top). (**G**) Scatter plot of the puncta index average (7-9 neurons per condition, Mann Whitney, *$p \leq 0.05$, ±SEM) for GFP-AnkG-190 or GFP-AnkG-190-C70A overexpression.

Figure 3. Lithium induces a decrease of palmitoylated AnkG-190 isoform and increases its mobility. (**A**) Lysates of cortical neurons treated with the indicated compounds were subjected to ABE to purify palmitoylated proteins. Levels of palmitoyl-AnkG-190 (top blot) and total AnkG expression in parent lysates (bottom blot) were detected with specific antibodies. Exclusion of NH_2OH was used as a control for assay specificity. (**B**) Bar graph of 190 kDa AnkG isoform palmitoylation normalized with the input and relative to the untreated condition (5 independent experiments, t-test, *$p \leq 0.05$, ±SEM). (**C**) Representative maximal projection of confocal image of endogenous AnkG staining in cortical neurons transfected with GFP with or without lithium stimulation, scale=2 µm. (**D**) Scatter plot of AnkG mean intensity in mushroom spines on a single plane (26-30 neurons on 3 independent experiments, t-test, ***$p \leq 0.001$, ±SEM). (**E**) Representative time lapse images of GFP-AnkG-190 fluorescence in 24 days rat neurons culture overexpressing GFP-AnkG-190 o GFP-AnkG-19-C70A for 3 day +/- lithium chloride during 1 day in FRAP experiments, scale=2 µm. (**F**) Quantification of GFP fluorescence in spines over time. Data are fitted with single exponentials (colored lines). Data are represented as mean ±SEM. (**G**) Scatter plots of mobile fraction (left) or half time recovery (right) of GFP-AnkG-190 or GFP-AnkG-190-C70A +/- lithium chloride (n=15-22 neurons, 1-ANOVA with Dunnett's post-test, ***$p \leq 0.001$)

Figure 4. Lithium prevents DHHC8 to stabilize AnkG-190 in dendritic spines.
(**A**) Representative time lapse images of GFP-AnkG-190 fluorescence in 24 days rat neurons culture overexpressing GFP-AnkG-190 with or without DHHC5 or DHHC8 during 3 days in FRAP experiments, scale=2 µm. Cultures are treated with palmostatin B +/- lithium chloride 24 hours prior the experiment (**B**) Quantification of GFP fluorescence in spines over time. Data are fitted with single exponentials (colored lines). Data are represented as mean ±SEM. (**C**) Scatter plots of mobile fraction (left) or half time recovery (right) of GFP-AnkG-190 in the presence or absence of ZDHHC5 +/- lithium chloride (n=8-10 neurons, 1-ANOVA with Dunnett's post-test). (**D**) Quantification of GFP fluorescence in spines over time. Data are fitted with single exponentials (colored lines). Data are represented as mean ±SEM. (**E**) Scatter plots of mobile fraction (left) or half time recovery (right) of GFP-AnkG-190 in the presence or absence of ZDHHC8 +/- lithium chloride (n=8-10 neurons, 1-ANOVA with Dunnett's post-test, *$p \leq 0.05$)

Figure 1

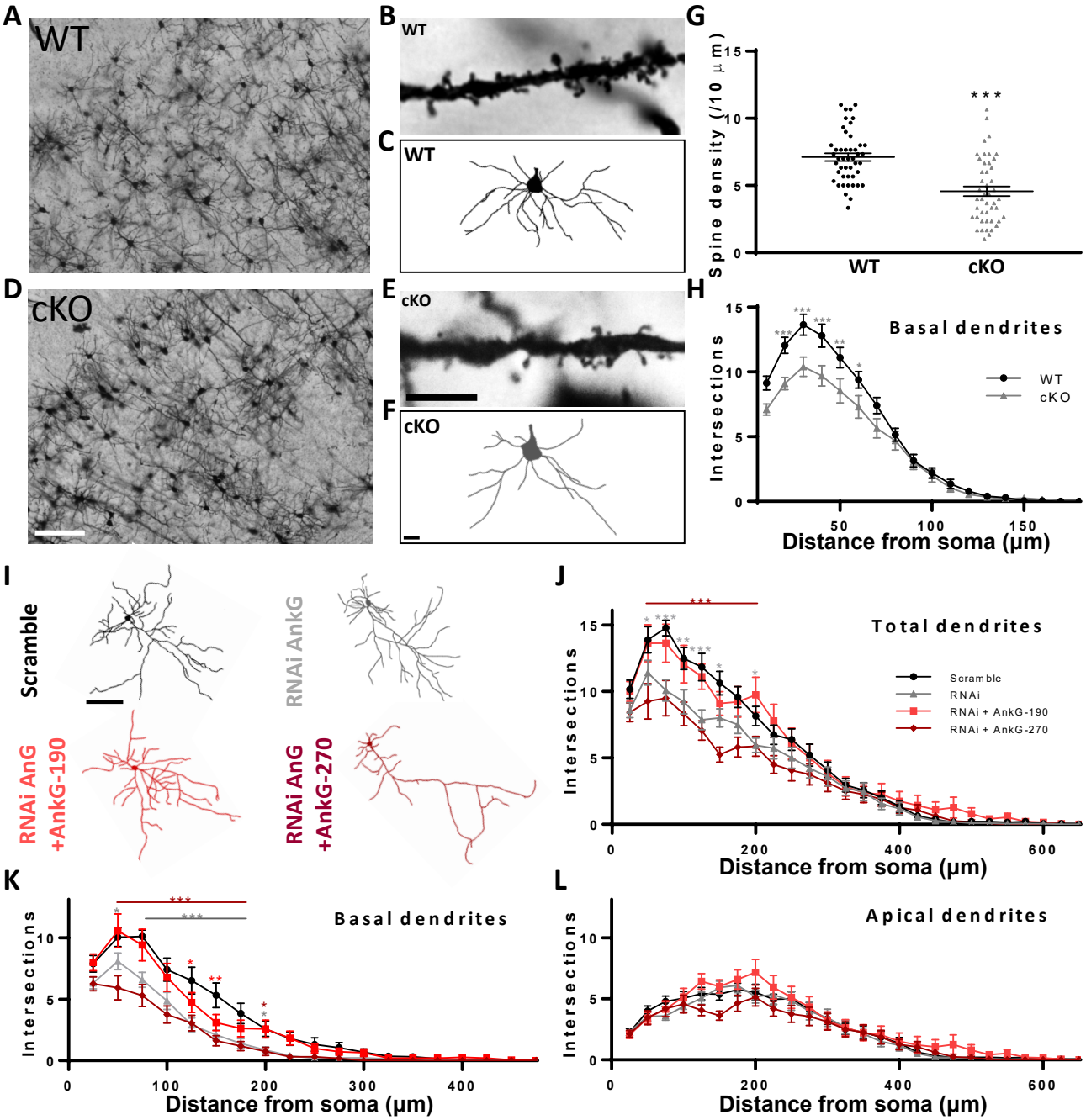
A
WT
B
WT
C
WT
D
cKO
E
cKO
F
cKO
G
Spine density (/10 μm)
***
WT
cKO
H
Basal dendrites
Intersections
WT
cKO
Distance from soma (μm)
I
Scramble
RNAi AnkG
RNAi AnG +AnkG-190
RNAi AnG +AnkG-270
J
Total dendrites
Intersections
Scramble
RNAi
RNAi + AnkG-190
RNAi + AnkG-270
Distance from soma (μm)
K
Basal dendrites
Intersections
Distance from soma (μm)
L
Apical dendrites
Intersections
Distance from soma (μm)

Figure 2

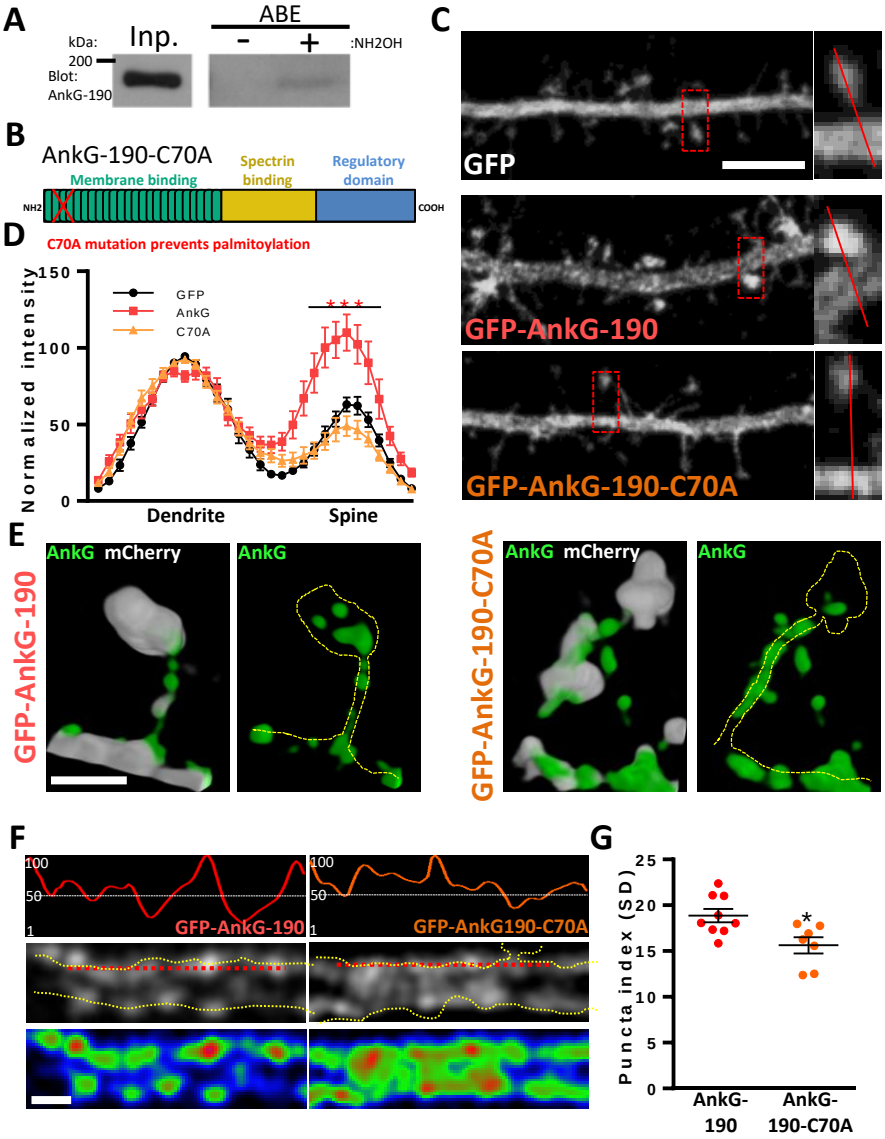
A
ABE
kDa:
Inp.
-
+
:NH2OH
200
Blot:
AnkG-190
B
AnkG-190-C70A
Membrane binding
Spectrin binding
Regulatory domain
NH2
COOH
C
GFP
GFP-AnkG-190
GFP-AnkG-190-C70A
D
C70A mutation prevents palmitoylation
Normalized intensity
150
100
50
0
GFP
AnkG
C70A
***
Dendrite
Spine
E
GFP-AnkG-190
AnkG mCherry
AnkG
GFP-AnkG-190-C70A
AnkG mCherry
AnkG
F
100
50
1
GFP-AnkG-190
GFP-AnkG190-C70A
G
Puncta index (SD)
25
20
15
10
5
0
*
AnkG-190
AnkG-190-C70A

Figure 3

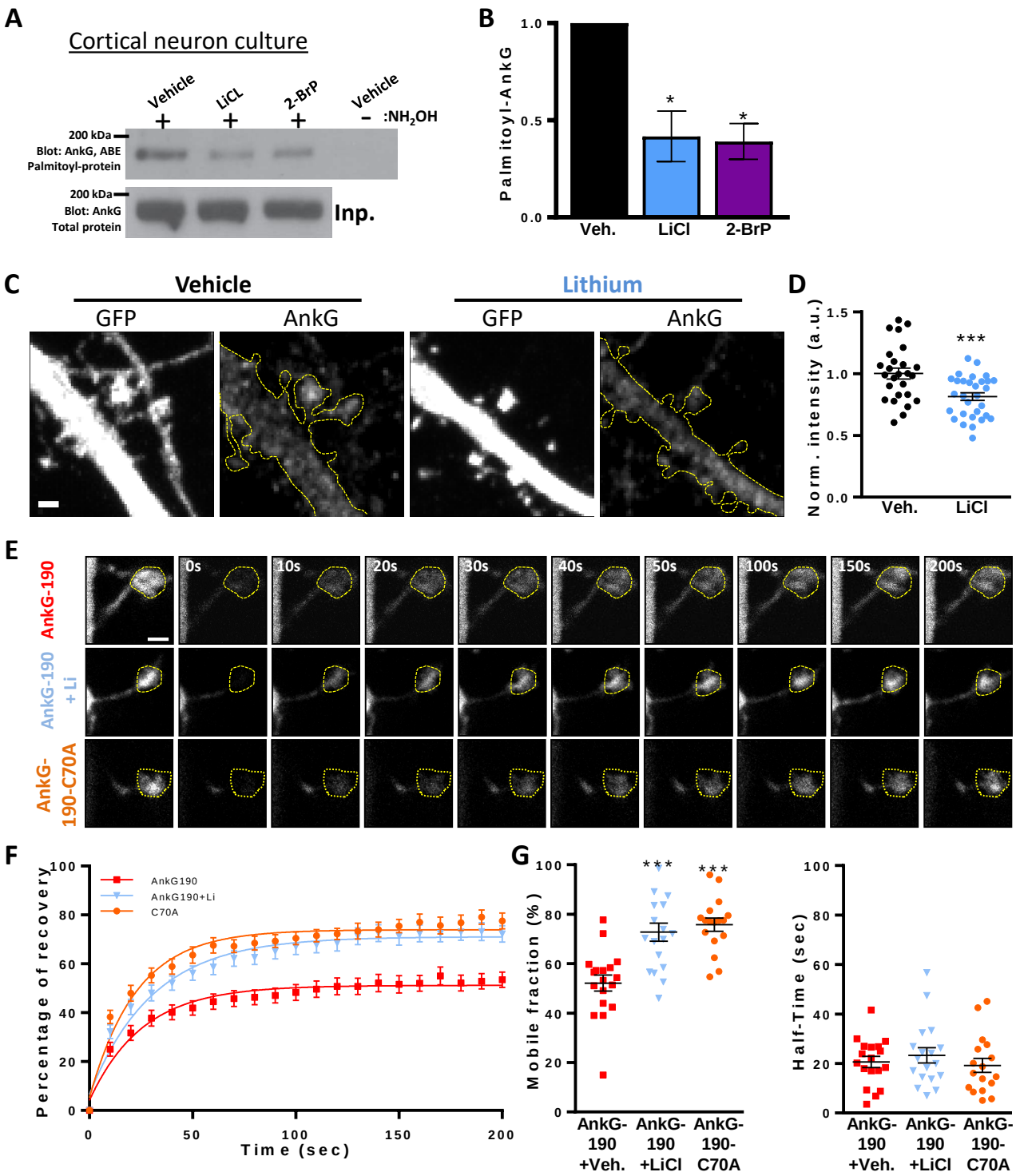
A
Cortical neuron culture
Vehicle
LiCL
2-BrP
Vehicle
+
+
+
– :NH2OH
200 kDa
Blot: AnkG, ABE
Palmitoyl-protein
200 kDa
Blot: AnkG
Total protein
Inp.
B
Palmitoyl-AnkG
1.0
0.5
0.0
*
*
Veh.
LiCl
2-BrP
C
Vehicle
Lithium
GFP
AnkG
GFP
AnkG
D
Norm. intensity (a.u.)
1.5
1.0
0.5
0.0
***
Veh.
LiCl
E
AnkG-190
AnkG-190 + Li
AnkG-190-C70A
0s
10s
20s
30s
40s
50s
100s
150s
200s
F
Percentage of recovery
AnkG190
AnkG190+Li
C70A
Time (sec)
G
Mobile fraction (%)
***
***
AnkG-190 +Veh.
AnkG-190 +LiCl
AnkG-190-C70A
Half-Time (sec)
AnkG-190 +Veh.
AnkG-190 +LiCl
AnkG-190-C70A

Figure 4

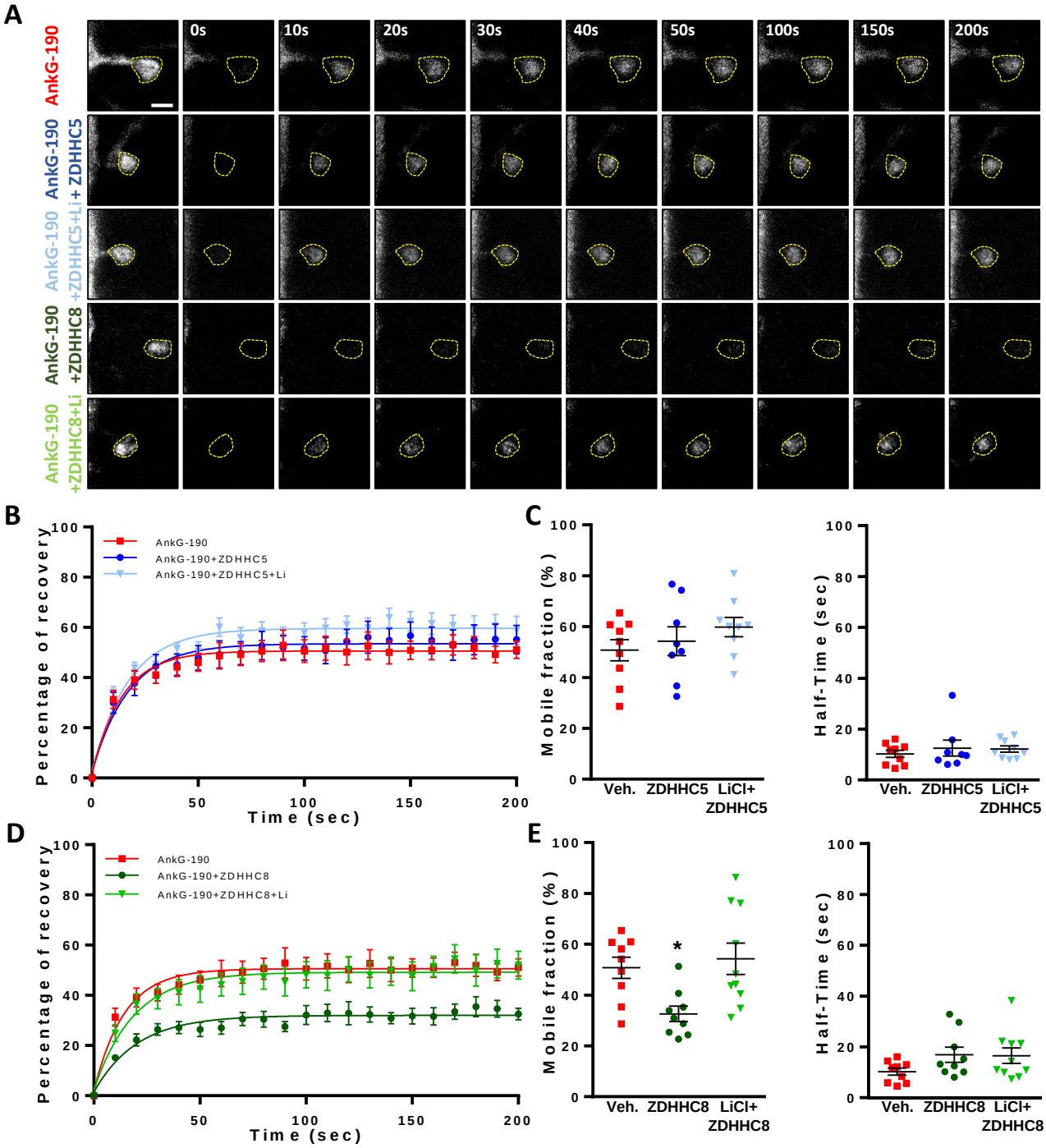
A
AnkG-190
AnkG-190 + ZDHHC5
AnkG-190 +ZDHHC5+Li
AnkG-190 +ZDHHC8
AnkG-190 +ZDHHC8+Li
0s
10s
20s
30s
40s
50s
100s
150s
200s
B
Percentage of recovery
Time (sec)
AnkG-190
AnkG-190+ZDHHC5
AnkG-190+ZDHHC5+Li
C
Mobile fraction (%)
Half-Time (sec)
Veh.
ZDHHC5
LiCl+ ZDHHC5
D
Percentage of recovery
Time (sec)
AnkG-190
AnkG-190+ZDHHC8
AnkG-190+ZDHHC8+Li
E
Mobile fraction (%)
Half-Time (sec)
Veh.
ZDHHC8
LiCl+ ZDHHC8
*